The relationship between blood flow impairment and oxygen depletion in acute ischemic stroke imaged with magnetic resonance imaging

Alexander Seiler[1], Nicholas P Blockley[2], Ralf Deichmann[3], Ulrike Nöth[3], Oliver C Singer[1], Michael A Chappell[2,4], Johannes C Klein[5] and Marlies Wagner[6]

Abstract

Oxygenation-sensitive spin relaxation time T2′ and relaxation rate R2′ (1/T2′) are presumed to be markers of the cerebral oxygen extraction fraction (OEF) in acute ischemic stroke. In this study, we investigate the relationship of T2′/R2′ with dynamic susceptibility contrast-based relative cerebral blood flow (rCBF) in acute ischemic stroke to assess their plausibility as surrogate markers of the ischemic penumbra. Twenty-one consecutive patients with internal carotid artery and/or middle cerebral artery occlusion were studied at 3.0 T. A physiological model of the cerebral vasculature (VM) was used to process PWI raw data in addition to a conventional deconvolution technique. T2′, R2′, and rCBF values were extracted from the ischemic core and hypoperfused areas. Within hypoperfused tissue, no correlation was found between deconvolved rCBF and T2′ ($r = -0.05$, $p = 0.788$), or R2′ ($r = 0.039$, $p = 0.836$). In contrast, we found a strong positive correlation with T2′ ($r = 0.444$, $p = 0.006$) and negative correlation with R2′ ($r = -0.494$, $p = 0.0025$) for rCBF$_{VM}$, indicating increasing OEF with decreasing CBF and that rCBF based on the vascular model may be more closely related to metabolic disturbances. Further research to refine and validate these techniques may enable their use as MRI-based surrogate markers of the ischemic penumbra for selecting stroke patients for interventional treatment strategies.

Keywords

Brain imaging, magnetic resonance imaging, oxygen metabolism, perfusion-weighted imaging, tissue at risk

Received 9 May 2017; Revised 23 August 2017; Accepted 24 August 2017

Introduction

In acute ischemic stroke, the concept of a tight coupling of cerebral blood flow (CBF) reduction and increase of cerebral oxygen extraction fraction (OEF) within the still viable tissue at risk of infarction (ischemic penumbra)[1–3] has led to growing research on oxygen-sensitive magnetic resonance imaging (MRI) techniques,[4–6] especially because widely used perfusion-weighted imaging (PWI) parameters including time-to-peak (TTP) and mean transit time (MTT) maps alone cannot be used to discriminate between real tissue at risk (ischemic penumbra) and benign oligemia reliably.[7,8] Apart from inherent technical issues of PWI, this problem is due to the fact that perfusion maps used in ischemic stroke only depict different degrees of perfusion impairment without considering metabolic factors including

[1]Department of Neurology, Goethe University Frankfurt, Frankfurt, Germany
[2]Nuffield Department of Clinical Neurosciences, Oxford Center for Functional MRI of the Brain, University of Oxford, Oxford, UK
[3]Brain Imaging Center, Goethe University Frankfurt, Frankfurt, Germany
[4]Department of Engineering Science, Institute of Biomedical Engineering, University of Oxford, Oxford, UK
[5]Nuffield Department of Clinical Neurosciences, Oxford University, and Department of Neurology, Oxford University Hospitals NHS Trust, Oxford, UK
[6]Institute of Neuroradiology, Goethe University Frankfurt, Frankfurt, Germany

The last two authors contributed equally to this work.

Corresponding author:
Alexander Seiler, Department of Neurology, Goethe University Frankfurt, Schleusenweg 2-16, Frankfurt am Main 60528, Germany.
Email: Alexander.Seiler@kgu.de

OEF that characterize the ischemic penumbra.[8] Although the infarct volume at admission has been shown to be the main determining factor of outcome after endovascular therapy,[9] a reliable image-based surrogate of the penumbra could be helpful for therapeutic decision-making,[10] e.g. when the time of symptom onset is not known or when patients display transient or fluctuating symptoms despite a persistent vessel occlusion.

Quantitative T2′ and R2′ (1/T2′) mapping, where T2′ basically represents the effective transverse relaxation time (T2*), corrected for spin-spin effects ($1/T2' = 1/T2* - 1/T2$), are sensitive to locally increased concentrations of paramagnetic deoxygenated hemoglobin (Hb).[11,12] A shift in global Hb ratio towards elevated concentrations of deoxygenated Hb results in a decrease/increase of T2′/R2′, respectively. Theoretically, R2′ (1/T2′) should be proportional to the product of relative OEF and relative cerebral blood volume (rCBV) multiplied with a tissue-specific constant[13] and thus be suitable to detect OEF increases. Significantly decreased T2′ values have been reported within hypoperfused tissue with delayed TTP in acute ischemic stroke. These data were interpreted as the consequence of increased OEF due to impaired perfusion.[14,15] While T2′ values were significantly decreased in the infarct core and the hypoperfused tissue, no correlation between T2′ and TTP delay could be found.[15] This suggested that the TTP delay alone is not an appropriate surrogate of cerebral OEF, and therefore does not allow for the differentiation between benign oligemia and penumbra in ischemic stroke. Even though TTP maps allow for rapid delineation of perfusion abnormalities by indicating any delay in arterial input and dispersion of the bolus, they provide rather unspecific information regarding local tissue perfusion. Consequently, CBF as the actual promoter of OEF alterations – which are assumed to cause T2′ changes – may show large variability within hypoperfused areas with TTP delay.[16]

The calculation of relative (r)CBF values from dynamic susceptibility contrast (DSC) imaging which depends on scaling factors determined by the postprocessing algorithm underlies some complexities and potential sources of error in raw data postprocessing. First, the widespread deconvolution techniques are prone to a high level of noise (yielding a low signal-to-noise ratio, SNR) which is generally present in the concentration-time curves obtained from DSC-MRI. Consequently, the tissue response (residue) function produced by deconvolution is naturally irregular.[17] Furthermore, the usual occurrence of a delay between the arterial input function (AIF) and the observed concentration-time curve can be problematic for DSC-MRI analysis. All these factors may result in an underestimation of rCBF and raise problems for the estimation of flow heterogeneity in DSC-MRI, particularly at low SNR.[17] The reliability of DSC-based rCBF can be improved by using for the calculations a physiological model of the perfusion dynamics of the cerebral microvasculature which produces a smoother, monotonically decreasing estimate of the residue function and is more robust to the delay between the AIF and the tissue concentration-time curve.[17,18] Those maps might be used to assess an rCBF decrease in acute large vessel occlusion more reliably. Furthermore, if it can be shown that there is a correlation between CBF reduction and decrease of T2′ as a marker of increased OEF in ischemic stroke, CBF alone could be used to better distinguish between oligemia and penumbra than TTP maps that are currently used in clinical routine.

In this study, rCBF together with T2′/R2′ in ischemic brain tissue during acute cerebral artery occlusion was investigated as a surrogate of the ischemic penumbra. It should be stressed that these data comprise high-resolution T2′/R2′ maps and DSC-based PWI data acquired on a highly selected patient collective with acute cerebral artery occlusion prior to revascularization procedures (intravenous thrombolysis and/or endovascular thrombectomy). Data to assess the relationship between oxygen-sensitive T2′/R2′ and rCBF were acquired in the acute phase of ischemic stroke by combining conventional PWI data with quantitative maps of T2 and T2* to calculate the oxygen-sensitive relaxation parameters T2′/R2′, following motion-correction with a custom-built algorithm. Because of the limited validity of conventionally generated rCBF-maps that are based on singular value deconvolution, a potentially more reliable method for obtaining the rCBF from DSC perfusion data was used. The combination of oxygen-sensitive parameters with blood flow measurements aimed at the confirmation that these methods may enable non-invasive assessment of the ischemic penumbra in acute ischemic stroke. Thus, the study is a contribution to the overall effort to investigate oxygen metabolism with MRI methods exploiting the blood oxygen level dependent (BOLD) contrast which is based on the susceptibility differences between deoxyhemoglobin and oxyhemoglobin.[4,6]

Materials and methods

Patients

Twenty-one consecutive patients with acute stroke due to proximal artery occlusion of the anterior circulation were included in this prospective study within the study period (June 2013 to December 2014). Parts of this patient population as well as the inclusion criteria

were described in more detail and published previously.[15] Written informed consent was obtained from each patient or their legal representative before inclusion in the study. All patients received intravenous thrombolysis after the exclusion of intracerebral hemorrhage and other contraindications. The study was approved by the Institutional Review Board of the medical faculty of the Goethe University (approval number: 275/12) and was performed in accordance with the Declaration of Helsinki. Potential eligibility for thrombectomy was evaluated using a standardized MRI protocol.

MR imaging protocol

MRI data were acquired on a 3 Tesla whole-body scanner (Magnetom Verio 3 T; Siemens Healthcare, Erlangen, Germany), equipped with a body transmit and an eight-channel phased array head receive coil. The total measurement time was 20:51 min. Data acquisition followed a protocol described previously.[15]

Diffusion-weighted images (DWI) were acquired with a single-shot spin-echo echo-planar imaging (EPI) sequence, using the following parameters: echo time $TE = 88$ ms, repetition time $TR = 4900$ ms, field-of-view (FOV) 220×220 mm^2, matrix size 130×130, 25 axial slices, slice thickness 5 mm, inter-slice gap 0.5 mm, bandwidth $BW = 1425$ Hz/Px, and $b = 1000$ s/mm^2. ADC maps were calculated using the commercially available scanner software.

Perfusion-weighted images (PWI) were acquired with a DSC gradient-echo (GE) EPI sequence. Imaging parameters were $TE = 30$ ms, $TR = 1500$ ms, flip angle $FA = 90°$, FOV 230×230 mm^2, matrix size 128×128, 19 axial slices, slice thickness 4 mm, 1.2 mm inter-slice gap, $BW = 1447$ Hz/Px. The intravenous contrast agent gadobutrol (0.1 mmol/kg; Gadovist$^®$ Bayer) was automatically applied by a power injector at a flow rate of 5 mL/s, followed by a bolus (20 mL) of 0.9% saline. The scanner software package was used to calculate TTP maps.

The sequence for quantitative T2* mapping has been described in detail in Noth et al.[19] In summary, a multi-slice, multi-GE sequence was used that samples a total of eight GE per excitation via successively inverting the readout gradient. Echoes were sampled under the same readout gradient polarity to avoid artifacts. Imaging parameters were: linear TE increase from 10 to 52 ms with a constant increment of 6 ms, $TR = 1500$ ms, $FA = 30°$, FoV 240×180 mm^2, matrix size 192×144 (readout $\times$ phase encoding), 25 axial slices, slice thickness 2 mm, no inter-slice gap, $BW = 299$ Hz/Px, measurement time 3:36 min. For the suppression of motion artifacts, this acquisition was repeated twice with reduced spatial resolution and thus restricted k-space coverage in phase encoding direction and six initial dummy scans to achieve steady state conditions. In detail, the first (second) repetition covered 50% (25%) of central k-space lines and had a measurement time of 1:57 min (1:03 min).

For quantitative T2 mapping, a turbo spin-echo sequence with four different TE values was used. Geometrical parameters (FoV, matrix size, slice number, thickness, and gap) were identical to the T2* protocol with full k-space coverage as listed above. To speed up data acquisition, the turbo spin-echo sequence acquired per excitation 11 spin echoes with different phase encoding via sending a series of refocusing pulses with a spacing of 16 ms. No other acceleration techniques were used. Further sequence parameters were $TR = 4670$ ms, $BW = 100$ Hz/Px, 180° refocusing pulses. Four data sets were acquired, where the echo covering central k-space occupied either the first, fourth, sixth, or eighth position in the echo train, thus yielding TE values of 16, 64, 96, and 128 ms.

Image processing and analysis

To reduce subject (head) motion artifacts, images for T2* mapping were subjected to a previously described motion artifact suppression algorithm.[19] T2′ maps were calculated as previously explained in detail.[15] R2′ maps were calculated applying the relationship $1/T2' = R2'$. Voxels with a large fraction of cerebrospinal fluid (CSF) were excluded by applying an empirical upper threshold of ≤ 300 ms to the T2′ maps, nulling all voxels beyond this value. Accordingly, for the R2′ maps, a lower threshold of ≥ 3.33 s^{-1} was chosen.

All data were skull-stripped using "BET"[20] which is part of FSL (FMRIB Software Library, http://www.fmrib.ox.ac.uk). DWI data were linearly coregistered to the T2* maps using "FLIRT."[21] As the ADC maps intended for further analysis do not provide sufficient anatomic contrast for precise coregistration, the first diffusion-weighted image ($b = 0$, purely T2-weighted) was coregistered to the first T2*-weighted image. Afterwards, the resulting coregistration matrix was applied to the ADC map. Since all images were acquired in an emergency setting, thus being potentially affected by subject movement during the scanning process, the four-dimensional (4D) PWI raw data were retrospectively motion-corrected, using "MCFLIRT"[21] prior to coregistration in order to minimize the impact of motion-related artifacts on the perfusion maps. Apart from motion correction, this tool was used to calculate parameter maps based on mean value, standard deviation, and signal variance across the entire perfusion time series. For coregistration, the first three volumes were extracted from the T2*-weighted time series using FSL ROI, since these could
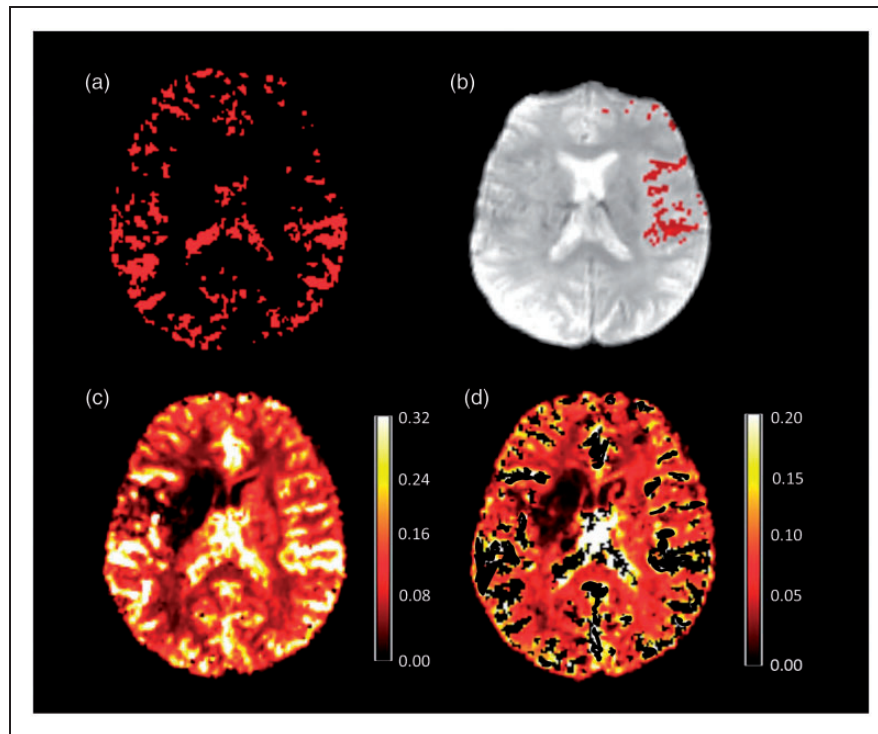
Figure 1. (a) Mask depicting the large vessels based on signal variance across time in the PWI time series. This mask was reduced to the anterior circulation of the unaffected side (b) in order to select voxels for the determination of the AIF shape. These voxels overlaid on the PWI raw data (b) show good agreement with the MCA branches of the Sylvian segment and the cortical branches (M2 and M3 segment). (c) rCBF map after processing of PWI raw data using the vascular model. Note that after correction for macrovascular components and applying the vessel mask, high-flow components reflecting large arterial vessels are removed (d) as indicated by the scale bars (c, d). rCBF values are given as non-dimensional numbers as exported by 'VERBENA'.

be assumed to provide adequate contrast between grey and white matter for coregistration. The mean value of these three volumes was calculated using FSL maths and used for linear coregistration to the T2* reference of the T2* mapping. The coregistration matrix of this step was saved and used for coregistering the final perfusion maps to the T2* data.

In order to reliably determine the shape of the AIF, voxels containing large arteries had to be extracted from the PWI time series. In a first step, the T2*-weighted time series were thresholded by applying a lower threshold of 70% of maximum signal intensity to the time series, using FSL maths. Afterwards, the standard deviation maps obtained with "MCFLIRT" were divided by the mean value maps to calculate coefficient of variation (CoV) maps. These CoV maps were thresholded using a lower threshold of 0.5, thus leaving voxels with a relatively high temporal signal intensity variation which is expected to indicate the presence of blood vessels. The threshold values had to be adjusted occasionally in order to retain a reasonable amount of voxels after the thresholding and masking procedure. A binary mask was created, based on the thresholded CoV map and used to mask the thresholded signal

intensity maps, yielding a map indicating areas of increased temporal signal variation for each patient (Figure 1(a)). Besides the cerebral arteries, these maps contained voxels belonging to cerebral veins and CSF. Therefore, a mask covering the basal frontal lobes, the basal cisterns, and the Sylvian fissure was created in standard space (MNI 152 2 mm, http://www.bic.mni. mcgill.ca/ServicesAtlases/) and used to mask out large cerebral veins and the ventricles. During the coregistration of the standard space vessel mask to the thresholded signal intensity mask, nearest neighbour interpolation was used to maintain the binary character of the mask. This procedure avoids reslicing the data which might affect parameter values due to interpolation effects. Finally, the resulting vessel masks were separated in the median plane to obtain artery masks for each side separately and used to mask the thresholded and masked time series. The final artery maps of the unaffected side (contralateral to the vessel occlusion) (Figure 1(b)) were used to determine the shape of the AIF. Using MATLAB, the mean value of all voxels in these artery maps along the fourth dimension (over time) was taken as a vector and subsequently, this vector was applied to every voxel of the
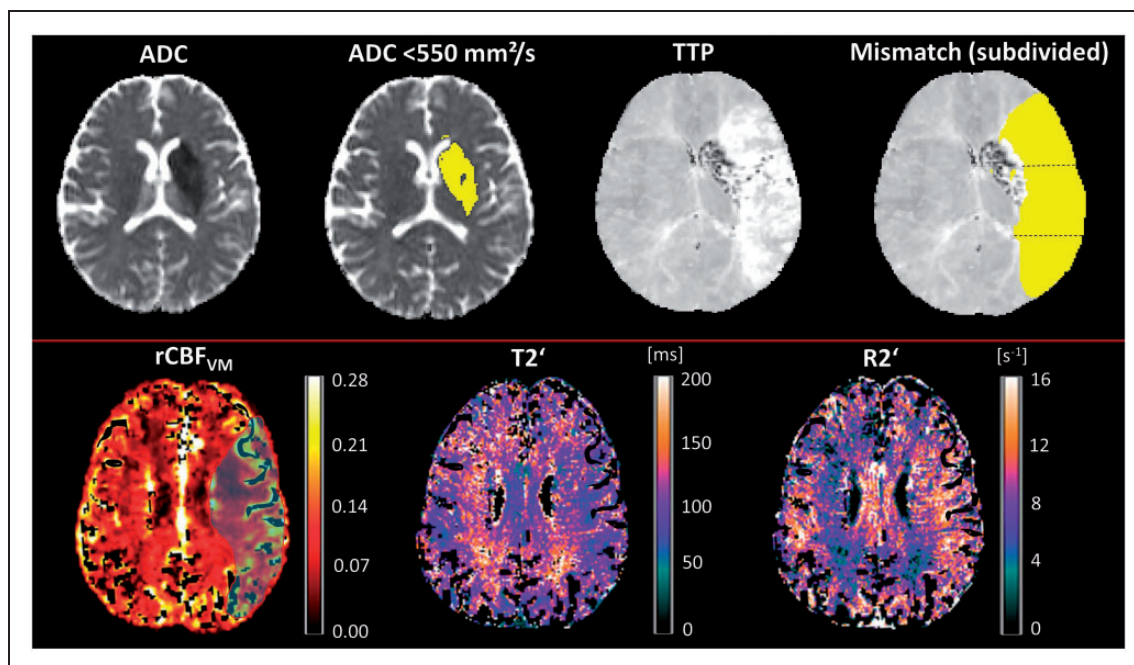
Figure 2. Upper row: illustration of ROI placement. The infarct core was defined as the hypointense areas on ADC maps with a threshold of $<550 \times 10^{-6}$ mm^2/s. The infarct core was subtracted from the TTP lesion to receive the DWI/PWI mismatch area that was further subdivided into three ROIs in anterior–posterior direction. Lower row: representative images of a patient from one slice above the ischemic core. The mask for the TTP lesion is overlaid on the rCBF map (light blue). rCBF values within this area are heterogeneous showing a clear reduction in the left periventricular white matter. T2′/R2′ map shows an area with decreased T2′/increased R2′ corresponding to the area of restricted flow. Correspondingly, T2′ is increased and R2′ decreased on the opposite side, indicating sufficient or high oxygen supply in well-perfused tissue. Parameter maps are corrected for large vessels as explained in the Methods section. ADC: apparent diffusion coefficient; mm: millimeters; s: seconds; TTP: time-to-peak; rCBF: relative cerebral blood flow; VM: vascular model; ms: milliseconds.

time series. As a consequence, many voxels used for the determination of the AIF were derived from the more distal parts (M2 and M3 segments) of the MCA. Compared to selecting voxels from the proximal part of the MCA, this approach has been shown to be advantageous concerning SNR and the reliability of values measured in DSC-based perfusion maps.[22] Finally, the resulting AIF was converted to a 4D file with uniform AIF for the whole brain to be used for processing the PWI raw data in order to generate rCBF maps using "VERBENA" which is part of the FSL toolbox.[18] The vascular model included in this tool produces a smooth, monotonically decreasing estimate of the residue function. Furthermore, the residue function estimate is characterized by only two parameters, which can be used to assess how the shape of the residue function varies among brain regions. In addition to the calculation of rCBF maps (Figure 1(c)) based on the vascular model, this tool was used to automatically correct for contamination with macrovascular components in voxels (e.g. caused by susceptibility effects of vessels nearby).[18] Finally, the blood vessel mask (Figure 1(a)) was used to remove larger blood vessels from the corrected rCBF maps (Figure 1(d)). Consequently, the

resulting maps predominantly contain information on rCBF within the microvasculature. To assess the differences between rCBF maps based on the vascular model (rCBF$_{VM}$) and conventional maps as used in clinical routine, rCBF maps were also generated based on singular value deconvolution (rCBF$_{SVD}$) using the scanner's software. AIFs for these maps were derived from two different sites frequently used in the clinical setting through selection of 5 to 10 voxels by an experienced neuroradiologist (M.W.): from the basal ganglia (tissue AIF) and the MCA trunk (vascular AIF) contralateral to the occlusion. Both rCBF$_{VM}$ and rCBF$_{SVD}$ maps were linearly coregistered to the T2* data.

T2′/R2′ and rCBF values were extracted from the ischemic core which was operationally defined by applying a threshold of $<550 \times 10^{-6}$ mm^2/s on the ADC maps (Figure 2, upper row) and the perfusion-restricted MCA-dependent territory defined by the TTP lesion (Figure 2, upper row). The latter was traced manually (A.S.). For maximal spatial coverage, ADC and TTP lesions were delineated in every slice using FSL view. In the case of overlapping lesions, the ADC lesion was subtracted from the PWI lesion for thorough separation of tissue compartments and to

receive the ADC/PWI mismatch area (Figure 2, upper row). To account for regional flow heterogeneity within the hypoperfused area, further regionalization of the TTP lesion was done by subdividing the lesion along the y-axis (anterior-posterior direction) into three relatively equally sized regions-of-interest (ROIs) with a rostral, a middle, and a dorsal ROI (Figure 2, upper row). This approach ensured the comparability between ROIs including relatively equal proportions of grey and white matter (that differ regarding $T2'/R2'$ values) while retaining the large ROIs that are required due to the relatively low SNR of $T2'/R2'$ maps. Furthermore, this method of regionalization with a territorial pattern respecting the distribution of leptomeningeal collaterals should allow for estimation of flow heterogeneity due to different degrees of collateralization. Mean rCBF and $T2'/R2'$ values of non-zero voxels (Figure 2, lower row) were extracted from all defined ROIs using FSL stats and compared to values from corresponding normoperfused areas after mirroring the ROIs to the contralateral side.

Data evaluation and assessment for artifacts

Since both quantitative imaging (especially T2*) and PWI are prone to artifacts induced by subject motion, we performed several analyses to evaluate data quality and to investigate the potential presence of misleading artifacts. First of all, an in-depth visual inspection of the quantitative raw data and the PWI time series was performed. Quantitative T2* maps were assessed for artifacts based on the correlation of T2* with the anatomical T2 reference and the dispersion of values around the mean (Supplementary material for details). For PWI, AIFs were selected for final analysis based on subjective criteria such as an early and steep drop in the signal time curve S(t), a limited amount of background noise, a smooth shape of the curve, and a quick signal return to baseline as these parameters contribute to a clearly discernible signal drop due to bolus-passage. The Supplemental Figure 1 shows an example for a representative patient. These characteristics were objectified by applying appropriate quantitative measures to the signal-time curves (Supplementary material for details).

Statistical analysis

Since the parameters were not normally distributed, only non-parametric statistical testing was used. The Wilcoxon-signed rank test was used to compare $T2'$, $R2'$, and rCBF between the defined ROIs inside the affected regions and inside the corresponding control areas of the unaffected hemisphere. Spearman's rank correlation was used for the evaluation of

parameter correlation. A value of $p < 0.05$ was considered significant. Statistical analysis was performed with SPSS 23 (IBM SPSS Statistics; SPSS Inc., Armonk, NY). Correction for multiple statistical testing using false discovery rate (FDR) correction was performed.

Results

Out of 21 patients, 15 patients provided PWI raw data and $T2'/R2'$ maps with a reasonable quality for further analysis, whereas six patients had to be excluded due to pronounced motion-related artifacts in the quantitative maps ($n = 4$) or insufficient bolus arrival on PWI ($n = 2$) (Supplementary material (Supplemental Table 1 and Supplemental Figures 2 to 5) for details). After further quantitative evaluation of the PWI data, a further four patients had to be excluded, due to insufficient peak salience and a high noise level in the 4D AIF file (Supplementary material (Supplemental Table 2 and Supplemental Figures 5 and 6) for details) that was used for calculation of $rCBF_{VM}$ maps in order to only include patients for which reliable $rCBF_{VM}$ data could be expected. Thus, 11 patients (four male, mean age 69 ± 12.9 years) were left for final analysis. A schematic overview of the different data processing steps and patient selection for final analysis is given in Figure 3. Mean time from symptom onset to MRI was 264 ± 63 min. Demographic and basic clinical data for each patient are given in Table 1.

The method of AIF selection did not significantly influence $rCBF_{SVD}$ values. Therefore, only the values calculated with the tissue AIF are given in the graphs. Changes of $T2'/R2'$ were most pronounced within the ischemic core and statistically significant for all ROIs. Mean values for $T2'/R2'$ and $rCBF_{VM}$ data are given in Table 2. Within the ischemic core, no significant correlation between $T2'/R2'$ and $rCBF_{VM}$ could be found ($r = -0.218$, $p = 0.519$ and $r = -0.018$, $p = 0.958$). In the entire mismatch area (TTP minus ADC lesion), a significant positive correlation between $T2'$ and $rCBF_{VM}$ ($r = 0.685$, $p = 0.01$, Figure 4(a)) and a significant negative correlation between $R2'$ and $rCBF_{VM}$ ($r = -0.685$, $p = 0.01$, Supplemental Figure 7(a)) were found. For $rCBF_{SVD}$, no significant correlations with either $T2'$ ($r = 0.327$, $p = 0.326$) or $R2'$ ($r = -0.327$, $p = 0.326$, Figure 4(b) and Supplemental Figure 7(b)) were found. When analyzing the relationship of $T2'/R2'$ and $rCBF_{VM}$ within the subdivided mismatch area, there was a strong significant positive correlation between $T2'$ and $rCBF_{VM}$ ($r = 0.444$, $p = 0.006$, Figure 4(c)) and a corresponding negative correlation between $R2'$ and $rCBF_{VM}$ ($r = -0.494$, $p = 0.0025$, Supplemental Figure 7(c)). Conventional $rCBF_{SVD}$ did not correlate with $T2'$ or $R2'$ ($r = -0.05$, $p = 0.788$
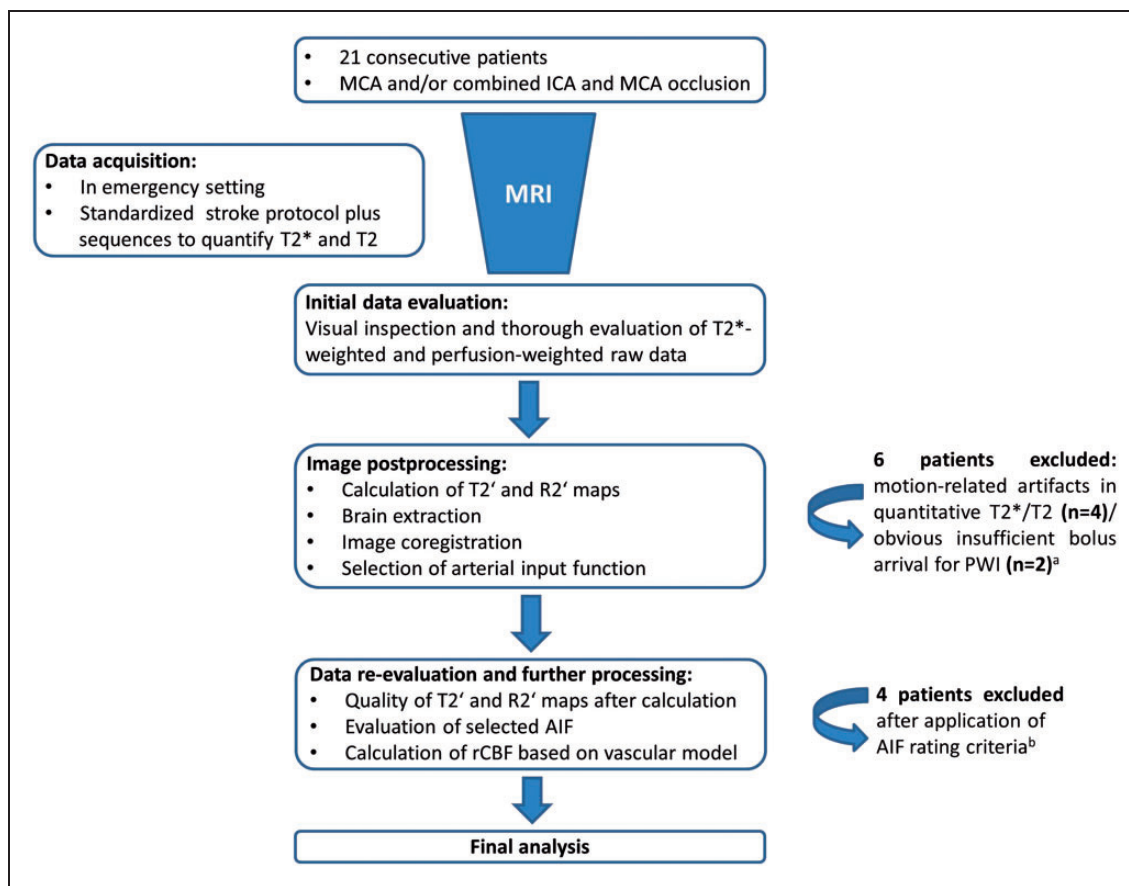
Figure 3. Flow diagram schematically illustrating the different steps of data analysis and selection for final analysis. (a) The methods applied for initial data evaluation and assessment for artifacts are explained in detail in the Supplementary material. (b) Quality of AIF was assessed based on different characteristics of the signal-time curves. Detailed descriptions of the methods and results can be found in the Supplementary material.

Table 1. Demographic and clinical baseline data.

Patient No.	Age, y/Sex	Affected hemisphere	Site of occlusion	Initial NIHSS	Onset-to-MRI time (min)
1	44/F	Left	ICA and MCA	30	238
2	69/M	Right	MCA M1	15	204
3	77/M	Right	MCA M1	14	300
4	72/F	Left	ICA and MCA	20	400
5	69/F	Left	MCA M1	17	272
6	84/F	Right	MCA M1	6	223
7	50/M	Right	ICA and MCA	12	256
8	82/M	Left	MCA M1	8	293
9	80/F	Right	ICA and MCA	18	191
10	60/F	Left	MCA M2	8	...
11	73/F	Left	MCA M1	6	...

Note: Exact time of symptom onset was not assessable in two patients. ICA: internal carotid artery; MCA: middle cerebral artery.

Table 2. Mean values (± standard deviations) for T2′/R2′ and rCBF_VM in the respective regions-of-interest and corresponding contralateral areas.

ROI	T2′ (ms)			R2′ (s⁻¹)			rCBF_VM		
	Affected	Unaffected	p	Affected	Unaffected	p	Affected	Unaffected	p
Ischemic core	88.07 ± 17.52	106 ± 14.62	0.004	14.48 ± 3.37	12.04 ± 2.26	0.01	0.047 ± 0.028	0.096 ± 0.039	0.004
Mismatch	92.94 ± 13.22	102.45 ± 14.19	0.01	10.97 ± 1.65	9.96 ± 1.41	0.01	0.072 ± 0.028	0.09 ± 0.033	0.005
Rostral	103.95 ± 8.22	114.05 ± 6.9	0.011	$12.36 \pm .37$	10.82 ± 1.06	0.021	0.068 ± 0.027	0.1 ± 0.037	0.008
Middle	100.58 ± 10.37	109.93 ± 11.01	0.01	12.29 ± 1.57	10.88 ± 1.2	0.003	0.065 ± 0.034	0.084 ± 0.035	0.01
Dorsal	99.02 ± 11.88	111.09 ± 10.89	0.004	12.25 ± 1.5	10.76 ± 1.08	0.004	0.086 ± 0.03	0.095 ± 0.034	0.026

ROI: region-of-interest; ms: milliseconds; s: seconds.
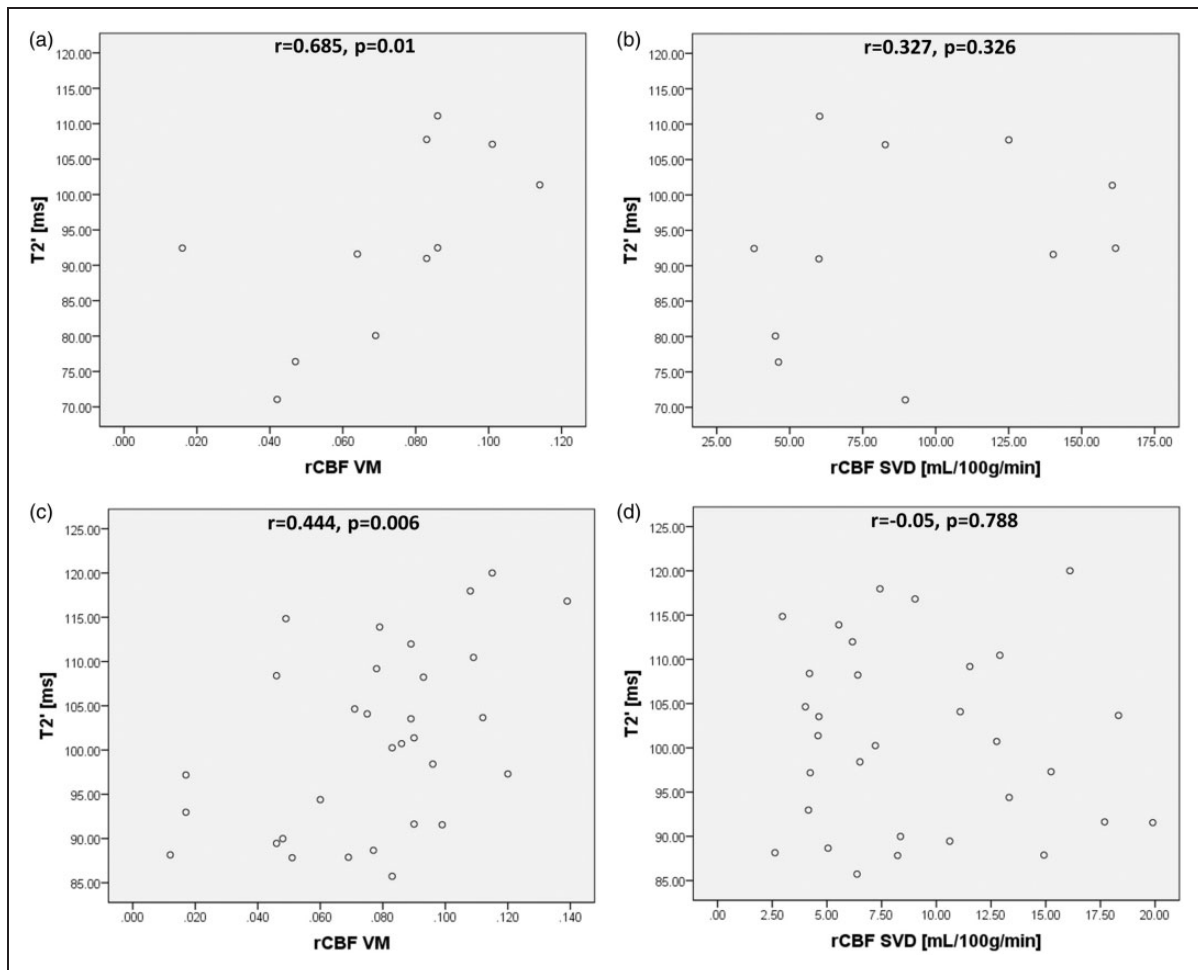
Figure 4. Scatterplots for T2′ values obtained from the entire (a, b) and the subdivided (c, d) mismatch area plotted against rCBF_VM and rCBF_SVD. Significant correlations were found between T2′ and rCBF_VM.
rCBF: relative cerebral blood flow; VM: vascular model; SVD: singular value deconvolution; ms: milliseconds; mL: milliliters; g: grams; min: minute.

and $r = 0.039$, $p = 0.836$, Figure 4 and Supplemental Figure 7, panels D). In general, the relative rCBF reduction within hypoperfused tissue as compared to the corresponding contralateral areas was lower for rCBF_VM than for rCBF_SVD ($22.46 \pm 17.82\%$ vs. $48.58 \pm 16.58\%$, $p = 0.0001$) (Supplemental Figure 8). FDR correction was performed for the respective parameters and the corrected level of significance was $p = 0.044$. Consequently, all results remained significant after FDR correction.

Discussion

This study examined the relationship between $T2'/R2'$ and rCBF, the latter being determined by applying both widely used SVD and a physiological model of the cerebral microvasculature. Although $T2'$ and $R2'$ can be expected to provide similar information, we measured both parameters in order to ensure comparability to previous studies. To the very best of our knowledge, this is the first study correlating oxygenation-sensitive motion-corrected $T2'$ and $R2'$ mapping with rCBF measurements in patients with acute large vessel stroke.

Endovascular therapy offers an opportunity for more individualized acute stroke treatment, yielding a therapeutic option for patients with symptom duration extending beyond conventional time windows. Besides a thorough evaluation of clinical symptoms, their dynamics over time and the vessel status, knowledge about the salvageable amount of tissue may be crucial for decision making in these situations. This requires estimation of oligemia and penumbra, which is defined by an increased OEF indicating metabolic stress.[2] The concept of the penumbra was established based on PET studies which found the OEF increase to be its hallmark.[2] Currently, efforts are made to develop MR parameters to measure the fraction of oxygen extracted from the blood. Although this fraction was not measured in this study, the term OEF is used to describe the underlying physiological processes for oxygenation changes in ischemic tissue.

TTP maps that can easily be obtained via the scanner's software have the advantage of rapidly providing information on perfusion delay in an affected territory – which we also used in the present study to delineate the vascular territory with an occluded source artery and to define the relevant ROIs. However, while TTP maps are frequently used in the clinical setting to estimate the amount of tissue at risk of infarction – usually by applying threshold values[23,24] – they do not supply reliable information on regional blood flow conditions.[16] Besides a regionally heterogeneous reduction of CBF in these areas, CBF in tissue around an occluded vessel might actually also be elevated due to increased perfusion via collaterals or in the case of early (partial) reperfusion.[16] Especially, the latter scenario may be masked by the delay of contrast input within the territory of an occluded artery and might therefore not be accounted for in TTP maps. Moreover, perfusion abnormalities as depicted by TTP maps have been shown to lack agreement with positron emission tomography (PET)-based OEF increases[7] as well as MRI-based surrogates of OEF elevations, namely $T2'$.[15] These findings suggest that a TTP delay does not necessarily indicate a CBF reduction which provokes a compensatory OEF increase if blood flow is

below the oligemic threshold. This suggests that through measuring $T2'/R2'$ in areas with TTP delay their potential to detect OEF increase is elucidated rarely and that a correlation with parameters that better reflect local hemodynamics and perfusion pressure is required, not only for judging pathophysiological plausibility of $T2'/R2'$ changes as surrogates of OEF elevations, but also for the implementation of techniques that allow for an improved estimation of penumbra and oligemia in the clinical setting. The physiological model of the cerebral vasculature used in this study is expected to allow for representation of blood flow heterogeneity.[25]

In this study, a significant positive correlation between $T2'$ and $rCBF_{VM}$ within the MCA-dependent territory was demonstrated. After further regionalization of the DWI/PWI mismatch region to analyze the association in more circumscribed compartments respecting heterogeneity of the respective parameters within the relatively large mismatch area, correlations with $rCBF_{VM}$ were significant for both $T2'$ and $R2'$, again showing a positive correlation between $T2'$ and $rCBF_{VM}$, while $R2'$ correlated negatively with $rCBF_{VM}$. These results suggest an incremental deoxygenation of Hb as the consequence of an elevated OEF with decreasing rCBF within the hypoperfused tissue, leading to higher concentrations of deoxygenated Hb and thus decreased $T2'$ and increased $R2'$. These results are in line with a previous study by Jensen et al.[26] that demonstrated a significant correlation of $T2'$ values and rCBF in a rat model of middle cerebral artery occlusion and reperfusion. Furthermore, a positive correlation of $T2'$ (negative for $R2'$) with DSC-based rCBV which is known to decrease as a linear function of rCBF in acute stroke,[27] has been shown in a previous work on patients with ICA and MCA occlusion.[28] Christen et al.[29] found a positive correlation of MR-derived $R2'$-based cerebral oxygen saturation measurements with both rCBF and rCBV in healthy subjects. Since these calculated oxygen saturation values are assumed to be reciprocally proportional to $R2'$,[29] the results obtained in this study can be considered as a confirmation of their findings under pathological conditions in relevantly hypoperfused brain tissue. Interestingly, conventional $rCBF_{SVD}$ values which generally showed a higher estimation of the degree of hemodynamic impairment (Supplemental Figure 2) did not correlate significantly with $T2'/R2'$ values (Figure 4(c) and (d)). This finding suggests that the vascular model streamlined to brain tissue and the cerebral microcirculation by correction for macrovascular components is more appropriate to reflect different degrees of local metabolic stress and alterations of OEF.

Our findings indicate that changes of $T2'$ and $R2'$ in ischemic stroke reflect alterations of OEF and are

closely related to the degree of blood flow impairment depicted by $rCBF_{VM}$ maps which might therefore be more appropriate to detect penumbral flow than commonly used TTP maps. Pathophysiologically, these findings are consistent with what had been reported in studies on stroke patients using PET, the gold standard for imaging of cerebral oxygen metabolism. A negative correlation with CBF in acute stroke was shown both for OEF (with multitracer investigation, amongst others using [15]O water)[30] and relative hypoxia as indicated by increased uptake of ^{18}F-Fluoromisonidazole (FMISO).[31] The fact that the most pronounced changes of T2′ and R2′ can be found in the ischemic core is presumably due to an almost complete blood deoxygenation as a consequence of highly impaired blood flow. As T2′/R2′ values also might be influenced to a certain extent by tissue iron content and fibre orientation,[32] ischemic necrosis with blood–brain barrier disruption, membrane disintegration, and axonal damage might have an additional influence and partially explain the repealed relationship of these parameters with rCBF in the ischemic core.

In summary, our study shows the close association between rCBF values based on the vascular model and T2′/R2′ as MRI-based surrogates of increased OEF in acute stroke providing pathophysiologically plausible results. Furthermore, the correlation of T2′ and R2′ with rCBF suggests rCBF as a more reliable parameter than TTP to estimate penumbra and oligemia in ischemic stroke. However, rCBF should be corrected for macrovascular components as performed in this study.

Limitations

This study has several limitations. Although the application of a postprocessing procedure for DSC data with the vascular model is advantageous in terms of avoidance of interpolation and theoretically should result in more reliable relative CBF data, displaying these data in dimensionless numbers makes it currently difficult to compare them to perfusion values obtained with established deconvolution methods. A validation of the vascular model against these conventional algorithms and PET measurements of cerebral perfusion will be required to judge their quantitative properties. As grey and white matter can be expected to differ in terms of infarction thresholds in DWI as well as viability thresholds for hypoperfusion and oxygen consumption, a segmentation of both the PWI and the T2′/R2′ data would be desirable. However, as anatomic imaging appropriate for segmentation is time-consuming, we did not acquire 3D T1-weighted sequences (e.g. MPRAGE) in our protocol to avoid delay of reperfusion therapy. It should be noted that a ROI-based approach was chosen for assessing potential correlations between T2′ and perfusion parameters. A voxel-wise approach was not deemed to be feasible as the T2′ maps are relatively noisy. This is due to the fact that R2′ is defined as the difference between R2* and R2. In the absence of major static magnetic field distortions, R2* will approach R2, so R2′ will tend towards zero, thus yielding erroneously high values of $T2′ = 1/R2′$. To avoid outliers, a maximum threshold of 300 ms was chosen for T2′ values. Even so, for T2* being close to T2, noise will have a marked impact on the resulting T2′ values which accounts for the reduced SNR in these maps. Consequently, the currently available T2′ maps cannot be used to directly delineate areas with certain ranges of T2′ values to determine thresholds of elevated deoxyhemoglobin concentration potentially defining the penumbra. Rather, this study confirms the pathophysiological assumptions associated with the use of the relaxation parameters T2′ and R2′ in ischemic stroke and encourages further research to improve these methods. However, at the current time-point, the immediate application as a clinical tool is not proposed, in view of the relatively high drop-out rate (about 50%). Nonetheless, it should be noted that high-resolution quantitative oxygenation-sensitive T2′/R2′ maps as used in this study are difficult to obtain in the setting of hyperacute stroke, thus necessitating improved postprocessing algorithms such as the proposed method. Additionally, the exclusion rate in this study is also the result of comprehensive data evaluation which was deemed necessary because of the sensitivity to artifacts and the complexity of determining rCBF with DSC. A validation of these findings with PET as the reference method for imaging oxygen metabolism in larger patient collectives would be of interest.

Conclusions

In conclusion, this study has shown the potential and pathophysiological plausibility of combining rCBF maps based on the vascular model with T2′ and R2′ mapping to detect local hypoperfusion and microvascular deoxygenation in acute ischemic stroke. Further research to refine and validate these techniques may enable their use as MRI-based surrogate markers of the ischemic penumbra for selecting stroke patients for interventional treatment strategies.

Declaration of conflicting interests

Authors' contributions

AS, NPB, RD, UN OCS, MAC, JCK, and MW designed the study. AS, RD, UN, OCS, and MW performed the MRI measurements. RD and UN developed the quantitative MRI sequences and the motion correction algorithm. MAC provided the tool used for the calculation of rCBF values based on the vascular model. AS, NPB, MAC, JCK, and MW analyzed the data and performed statistical analysis. AS, NPB, RD, UN OCS, MAC, JCK, and MW wrote the manuscript. JCK and MW contributed equally to this work.

Supplementary material

Supplementary material for this paper can be found at the journal website: http://journals.sagepub.com/home/jcb

References

1. Baron JC, Bousser MG, Comar D, et al. Noninvasive tomographic study of cerebral blood flow and oxygen metabolism in vivo. Potentials, limitations, and clinical applications in cerebral ischemic disorders. *Eur Neurol* 1981; 20: 273–284.

2. Baron JC. Mapping the ischaemic penumbra with PET: implications for acute stroke treatment. *Cerebrovasc Dis* 1999; 9: 193–201.

3. Heiss WD. Ischemic penumbra: evidence from functional imaging in man. *J Cereb Blood Flow Metab* 2000; 20: 1276–1293.

4. Jensen-Kondering U and Baron JC. Oxygen imaging by MRI: can blood oxygen level-dependent imaging depict the ischemic penumbra? *Stroke* 2012; 43: 2264–2269.

5. Dani KA and Warach S. Metabolic imaging of ischemic stroke: the present and future. *Am J Neuroradiol* 2014; 35: S37–S43.

6. An H, Ford AL, Vo KD, et al. Imaging oxygen metabolism in acute stroke using MRI. *Curr Radiol Rep* 2014; 2: 39.

7. Sobesky J, Zaro Weber O, et al. Does the mismatch match the penumbra? Magnetic resonance imaging and positron emission tomography in early ischemic stroke. *Stroke* 2005; 36: 980–985.

8. Sobesky J. Refining the mismatch concept in acute stroke: lessons learned from PET and MRI. *J Cereb Blood Flow Metab* 2012; 32: 1416–1425.

9. Goyal M, Menon BK, van Zwam WH, et al. Endovascular thrombectomy after large-vessel ischaemic stroke: a meta-analysis of individual patient data from five randomised trials. *Lancet* 2016; 387: 1723–1731.

10. Sobesky J. Leaving the black box approach: individualized prediction of recanalization benefit by advanced imaging in acute stroke. *J Cereb Blood Flow Metab* 2015; 35: 1396.

11. Wagner M, Jurcoane A, Volz S, et al. Age-related changes of cerebral autoregulation: new insights with quantitative T2'-mapping and pulsed arterial spin-labeling MR imaging. *AJNR Am J Neuroradiol* 2012; 33: 2081–2087.

12. Wagner M, Magerkurth J, Volz S, et al. T2'- and PASL-based perfusion mapping at 3 Tesla: influence of oxygen-ventilation on cerebral autoregulation. *J Magn Reson Imag* 2012; 36: 1347–1352.

13. Hirsch NM, Toth V, Forschler A, et al. Technical considerations on the validity of blood oxygenation level-dependent-based MR assessment of vascular deoxygenation. *NMR Biomed* 2014; 27: 853–862.

14. Geisler BS, Brandhoff F, Fiehler J, et al. Blood-oxygen-level-dependent MRI allows metabolic description of tissue at risk in acute stroke patients. *Stroke* 2006; 37: 1778–1784.

15. Bauer S, Wagner M, Seiler A, et al. Quantitative T2'-mapping in acute ischemic stroke. *Stroke* 2014; 45: 3280–3286.

16. Heiss WD and Zaro Weber O. Uncertainties in the assessment of cortical flow by perfusion-weighted MRI in acute stroke. *Cerebrovasc Dis* 2011; 32: 194–195; author reply 6.

17. Mouridsen K, Friston K, Hjort N, et al. Bayesian estimation of cerebral perfusion using a physiological model of microvasculature. *Neuroimage* 2006; 33: 570–579.

18. Chappell MA, Mehndiratta A and Calamante F. Correcting for large vessel contamination in dynamic susceptibility contrast perfusion MRI by extension to a physiological model of the vasculature. *Magn Reson Med* 2015; 74: 280–290.

19. Noth U, Volz S, Hattingen E, et al. An improved method for retrospective motion correction in quantitative T2* mapping. *Neuroimage* 2014; 92: 106–119.

20. Smith SM. Fast robust automated brain extraction. *Hum Brain Mapp* 2002; 17: 143–155.

21. Jenkinson M, Bannister P, Brady M, et al. Improved optimization for the robust and accurate linear registration and motion correction of brain images. *Neuroimage* 2002; 17: 825–841.

22. Ebinger M, Brunecker P, Jungehulsing GJ, et al. Reliable perfusion maps in stroke MRI using arterial input functions derived from distal middle cerebral artery branches. *Stroke* 2010; 41: 95–101.

23. Zaro-Weber O, Moeller-Hartmann W, Heiss WD, et al. MRI perfusion maps in acute stroke validated with 15O-water positron emission tomography. *Stroke* 2010; 41: 443–449.

24. Dani KA, Thomas RG, Chappell FM, et al. Computed tomography and magnetic resonance perfusion imaging in ischemic stroke: definitions and thresholds. *Ann Neurol* 2011; 70: 384–401.

25. Ostergaard L, Chesler DA, Weisskoff RM, et al. Modeling cerebral blood flow and flow heterogeneity from magnetic resonance residue data. *J Cereb Blood Flow Metab* 1999; 19: 690–699.

26. Jensen UR, Liu JR, Eschenfelder C, et al. The correlation between quantitative T2' and regional cerebral blood flow after acute brain ischemia in early reperfusion as

demonstrated in a middle cerebral artery occlusion/reperfusion model of the rat. *J Neurosci Meth* 2009; 178: 55–58.

27. Singer OC, de Rochemont Rdu M, Foerch C, et al. Relation between relative cerebral blood flow, relative cerebral blood volume, and mean transit time in patients with acute ischemic stroke determined by perfusion-weighted MRI. *J Cereb Blood Flow Metab* 2003; 23: 605–611.

28. Seiler A, Deichmann R, Noth U, et al. Oxygenation-sensitive magnetic resonance imaging in acute ischemic stroke using T2′/R2′ mapping: influence of relative cerebral blood volume. *Stroke* 2017; 48: 1671–1674.

29. Christen T, Schmiedeskamp H, Straka M, et al. Measuring brain oxygenation in humans using a multiparametric quantitative blood oxygenation level dependent MRI approach. *Magn Reson Med* 2012; 68: 905–911.

30. Sette G, Baron JC, Mazoyer B, et al. Local brain haemodynamics and oxygen metabolism in cerebrovascular disease. Positron emission tomography. *Brain* 1989; 112(Pt 4): 931–951.

31. Alawneh JA, Moustafa RR, Marrapu ST, et al. Diffusion and perfusion correlates of the 18F-MISO PET lesion in acute stroke: pilot study. *Eur J Nucl Med Mol Imag* 2014; 41: 736–744.

32. Sedlacik J, Boelmans K, Lobel U, et al. Reversible, irreversible and effective transverse relaxation rates in normal aging brain at 3T. *Neuroimage* 2014; 84: 1032–1041.